A point mutation in TRPC3 causes abnormal Purkinje cell development and cerebellar ataxia in moonwalker mice

Esther B. E. Becker[a,b], Peter L. Oliver[a,b], Maike D. Glitsch[b], Gareth T. Banks[c], Francesca Achilli[c], Andrea Hardy[d], Patrick M. Nolan[d], Elizabeth M. C. Fisher[c], and Kay E. Davies[a,b,1]

[a]Medical Research Council Functional Genomics Unit, [b]Department of Physiology, Anatomy and Genetics, University of Oxford, South Parks Road, Oxford OX1 3QX, United Kingdom; [c]Department of Neurodegenerative Disease, Institute of Neurology, University College London, Queen Square, London WC1N 3BG, United Kingdom; and [d]Medical Research Council Mammalian Genetics Unit, Harwell, Oxfordshire OX11 0RD, United Kingdom

Edited by Mary F. Lyon, Medical Research Council, Oxon, United Kingdom, and approved February 26, 2009 (received for review October 24, 2008)

The hereditary ataxias are a complex group of neurological disorders characterized by the degeneration of the cerebellum and its associated connections. The molecular mechanisms that trigger the loss of Purkinje cells in this group of diseases remain incompletely understood. Here, we report a previously undescribed dominant mouse model of cerebellar ataxia, moonwalker (*Mwk*), that displays motor and coordination defects and loss of cerebellar Purkinje cells. *Mwk* mice harbor a gain-of-function mutation (T635A) in the *Trpc3* gene encoding the nonselective transient receptor potential cation channel, type C3 (TRPC3), resulting in altered TRPC3 channel gating. TRPC3 is highly expressed in Purkinje cells during the phase of dendritogenesis. Interestingly, growth and differentiation of Purkinje cell dendritic arbors are profoundly impaired in *Mwk* mice. Our findings define a previously unknown role for TRPC3 in both dendritic development and survival of Purkinje cells, and provide a unique mechanism underlying cerebellar ataxia.

cerebellum | dendritogenesis | trp channel | mouse mutant

The inherited cerebellar ataxias are a complex group of neurodegenerative disorders characterized by loss of balance and coordination (1–3). Cerebellar ataxia is caused by the degeneration of Purkinje cells, which form the sole output of the cerebellum. To date, more than 50 different inherited forms of cerebellar ataxia are known (4). Importantly, increasing evidence points to the existence of common pathological pathways in different forms of ataxia, including transcriptional regulation, protein aggregation, and calcium homeostasis, which trigger the degeneration of Purkinje cells in these disorders (1, 5). However, the molecular mechanisms mediating these pathways remain poorly understood.

To identify gene products that might be key to cerebellar degeneration, we used a phenotype-driven approach to screen for ataxic behavior in a large cohort of *N*-ethyl-*N*-nitrosourea (ENU)-mutagenized mice (6). Here, we report that a point mutation (T635A) in the C3-type transient receptor potential (TRPC3) channel in the mouse results in Purkinje cell degeneration and cerebellar ataxia. We also find that the development of dendrites is severely impaired in mutant Purkinje cells. Notably, the identified dominant gain-of-function mutation in TRPC3 provides insight into the function of TRPC3 that powerfully complements the findings obtained from the recently published TRPC3 knockout mouse (7). Our findings suggest that TRPC3 is a regulator of development and survival of Purkinje cells, and link aberrant TRPC3 function to cerebellar disease.

Results

Moonwalker Mice Exhibit Impaired Motor and Coordination Control. We have identified a unique dominant ataxic mouse mutant, moonwalker (*Mwk*; Mouse Genome Informatics database accession no. 3689326), from a large-scale, phenotype-driven dominant mutagenesis screen (6). Heterozygous *Mwk* mice (*Mwk*/+) are generally 60% of the size of their wild-type littermates, which is commonly observed in ataxic mouse mutants, and display gait abnormalities including retropulsion from 3 weeks of age [supporting information (SI) Movie S1]. Homozygous mutants (*Mwk*/*Mwk*) are not viable. To characterize the ataxic behavior of *Mwk*/+ mice in more detail, we analyzed gait abnormalities of adult mutant mice and wild-type littermates from their footprint patterns. Wild-type mice walked along a straight line with a smooth alternating gait (Fig. 1*A*). In contrast, *Mwk*/+ mice meandered from side to side while moving with a significantly broader gait width (the lateral distance between opposite right and left footsteps) than their wild-type littermates (Fig. 1 *A* and *B*). Furthermore, mutant mice displayed a nonuniform alternating left-right step pattern or "shuffling gait" (Fig. 1 *A* and *C*). We further assessed motor coordination of *Mwk*/+ mice and controls in a static rod test (8). For this, mice were placed on the protruding end of a fixed rod, facing away, and the latency to fall off while turning around and reaching the supported end of the bar was recorded. We found that *Mwk*/+ mice were severely impaired in their ability to maintain their balance and walk across the beam (Fig. 1*D*). Together, these behavioral tests demonstrate substantial motor and coordination defects in *Mwk*/+ mice.

Purkinje Cell Loss in *Mwk* Mice. The abnormal motor behavior of *Mwk*/+ mice led us to histologically examine the cerebellum, which is the brain region essential for coordination and motor control. The general cerebellar structure of mutant mice was indistinguishable from those of littermate controls. However, from 4 months of age, *Mwk*/+ mice showed a slow but progressive loss of Purkinje cells, the neurons that generate the sole output of the cerebellar cortex. From 6 months of age, more extensive Purkinje cell loss was observed, particularly in the lateral cerebellar hemispheres (Fig. 2 *A–D*), consistent with the observed motor coordination deficits in the mutant mice. No significant change in the size of the cerebellar granule neuron layer was noted (Fig. S1).

The Mwk Mutation Lies Within the *Trpc3* Gene. To identify the mutation underlying the *Mwk* ataxic phenotype, we performed

Author contributions: E.B.E.B., M.D.G., P.M.N., E.M.C.F., and K.E.D. designed research; E.B.E.B., P.L.O., M.D.G., G.T.B., F.A., and A.H. performed research; E.B.E.B., P.L.O., M.D.G., G.T.B., and F.A. analyzed data; and E.B.E.B., P.L.O., M.D.G., and K.E.D. wrote the paper.

The authors declare no conflict of interest.

This article is a PNAS Direct Submission.

Freely available online through the PNAS open access option.

Data deposition: The sequence reported in this paper has been deposited in the Mouse Genome Informatics database (accession no. 3689326).

[1]To whom correspondence should be addressed. E-mail: kay.davies@dpag.ox.ac.uk.

This article contains supporting information online at www.pnas.org/cgi/content/full/0810599106/DCSupplemental.

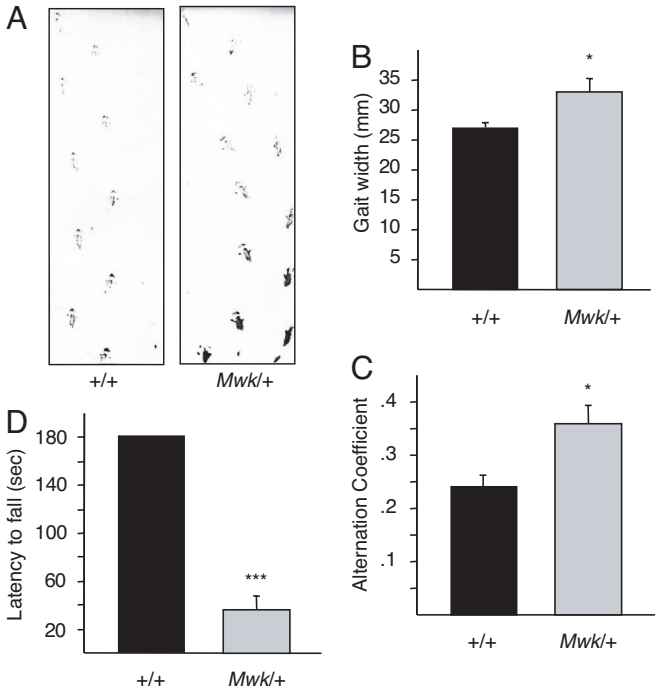

Fig. 1. Ataxic behavior in *Mwk*/+ mice. (*A*) Representative footprint patterns of wild-type and mutant mice at 2 months. Footprint patterns were quantitatively assessed for gait width (*B*) and step alternation uniformity (*C*). *Mwk*/+ mice displayed significantly wider gait (33 ± 2 mm vs. 27 ± 1 mm) and irregular step alternation (alternation coefficient 0.36 ± 0.035 vs. 0.24 ± 0.02) compared with wild-type controls (mean ± SEM, $n = 8$, $P < 0.05$, ANOVA followed by Fisher's PLSD post hoc test). (*D*) Static rod performance of wild-type and mutant mice at 2 months. *Mwk*/+ mice were significantly impaired in their ability to walk across the beam (35.7 ± 13.25 sec vs. 180 ± 0 sec; mean ± SEM, $n = 8$, $P < 0.0001$, ANOVA followed by Fisher's PLSD post hoc test).

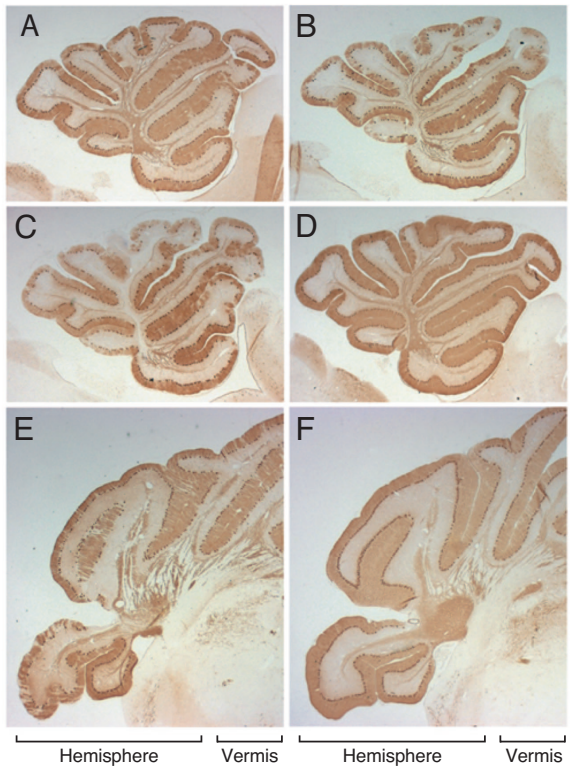

Fig. 2. Progressive Purkinje neuron loss in the *Mwk*/+ cerebellum. Calbindin-stained parasagittal sections from 6-month-old (*A*), 9-month-old (*B*), 12-month-old *Mwk*/+ (*C*), and wild-type mice (*D*). Coronal sections of 6-month-old *Mwk*/+ (*E*) and wild-type (*F*) mice show pronounced loss of Purkinje cells in the lateral cerebellar hemispheres of mutant mice.

a genome scan followed by fine mapping and haplotype analysis. We localized the *Mwk* mutation to a 4.9-Mb interval on mouse chromosome 3, flanked by *D3Mit206* and *D3Mit169*, containing 28 annotated genes (Ensembl release 50, July 2008). We then directly sequenced the coding regions and exon-intron boundaries of all genes in the nonrecombinant *Mwk* region. We identified a single nonsynonymous point mutation in exon 7 of the *Trpc3* gene, encoding the transient receptor potential cation channel, subfamily C, member 3 (TRPC3). No other mutations were found. The *Trpc3* transcript harbors an A-to-G transition at nucleotide position 1903 in *Mwk*/+ mice compared with the wild-type parental strains (Fig. 3*A*). The *Mwk* mutation causes a threonine-to-alanine amino acid change (T635A) in the highly conserved S4/S5 linker region of the TRPC3 protein (Fig. 3*B*). TRPC3 is a member of the canonical TRP subfamily of nonselective cation channels, which act as sensors of the cellular environment (9–12). Despite being the subject of intense scrutiny, the physiological role of TRPC3 remains largely unknown. Interestingly, TRPC3 is highly enriched in Purkinje cells in the cerebellum (7, 13) (Fig. 5 *A–D*), which is consistent with the observed specific cerebellar phenotype in *Mwk*/+ mice.

The mutation of a conserved residue in TRPC3 could interfere with the correct expression, folding, and/or targeting of the channel protein and thereby cause the disease phenotype in *Mwk*/+ mice. We detected similar levels of TRPC3 mRNA and protein in wild-type and mutant cerebellum (Fig. 3 *C* and *D*), suggesting that the mutated TRPC3 channel is expressed at similar levels as wild-type TRPC3. Furthermore, the cerebellar expression of TRPC1, another TRPC channel expressed in the cerebellum that is able to form heteromeric complexes with TRPC3 and contribute to Purkinje cell signaling (7, 14, 15), was not altered (Fig. 3*C*), suggesting that there is no functional compensation of mutant TRPC3 by TRPC1. In additional experiments, we showed that mutant TRPC3 localizes to similar vesicular structures as wild-type TRPC3 when transiently overexpressed (Fig. S2) (16). Thus, the *Mwk* mutation does not appear to alter the normal expression pattern of TRPC3 in the cerebellum.

Functional Consequences of the Mwk Mutation. TRPC3 is a key mediator of metabotropic glutamate receptor (mGluR)-dependent synaptic transmission in cerebellar Purkinje cells (7). We therefore assessed the inward currents evoked by application of the type 1 mGluR agonist (S)-3,5-dihydroxyphenylglycine (DHPG) in acute cerebellar slices of wild-type and *Mwk*/+ mice at P20–22, when the ataxic phenotype of the mutant mice is apparent. In wild-type slices, application of DHPG at a high concentration (20 μM) reproducibly produced an inward current and large spikes (Fig. 4*A*). In contrast, in *Mwk*/+ slices, the application of 20 μM DHPG resulted in an inward current with significantly smaller spikes at a faster interspike interval or no spikes at all (Fig. 4*B*). Interestingly, upon application of a low DHPG concentration (5 μM), there was hardly any or no inward current in wild-type Purkinje cells, but a clear inward current in *Mwk*/+ Purkinje cells (Fig. 4 *C* and *D*). Together, these findings suggest that the *Mwk* mutation results in altered TRPC3 gating that promotes channel opening under conditions of low mGluR1 activation.

Consistent with our findings that the *Mwk* mutation triggers abnormal TRPC3 channel opening, we found that the transient overexpression of mutant TRPC3 but not wild-type TRPC3

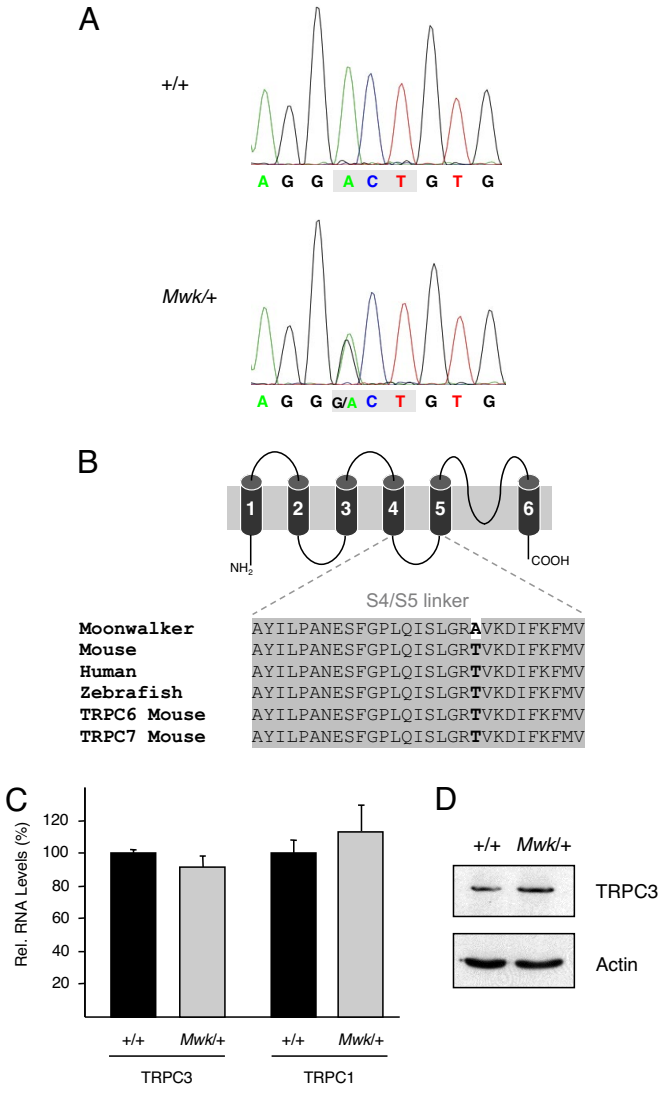

Fig. 3. The *Mwk* mutation is identified in the *Trpc3* gene. (*A*) Sequence analysis of the Trpc3 locus in wild-type and *Mwk*/+ DNA. An A1903G transversion was detected in *Mwk*/+ mice but was not present in the parental substrains. (*B*) Schematic of the 6-transmembrane TRPC3 channel protein. The expanded S4/S5 linker contains the *Mwk* mutation (T635A). Multiple amino acid sequence alignment of this region between orthologous TRPC3 and related (TRPC6, TRPC7) proteins from different mammalian species shows a very high degree of conservation. (*C*) TRPC3 and TRPC1 RNA levels normalized against calbindin RNA levels in cerebella from 3-week-old wild-type and *Mwk*/+ mice. (*D*) TRPC3 and actin protein levels in cerebellar lysates from 3-week-old wild-type and *Mwk*/+ mice.

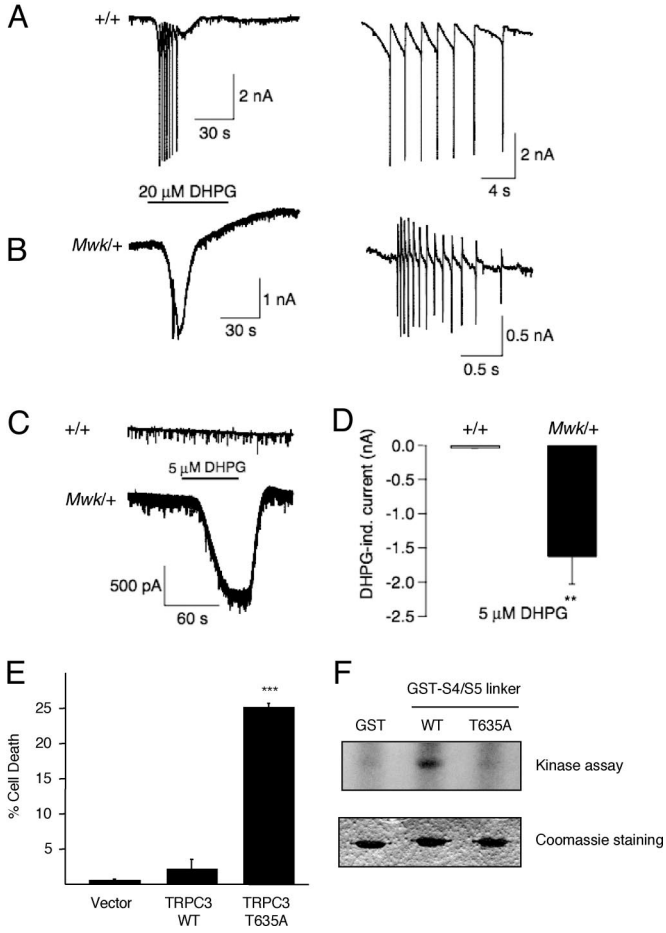

Fig. 4. The *Mwk* mutation results in altered TRPC3 phosphorylation and gating that promotes aberrant channel opening and cell death. Inward current in wild-type (*A*) and *Mwk*/+ (*B*) slices upon application of 20 μM DHPG. The spikes recorded in *Mwk*/+ Purkinje cells were significantly smaller and occurred at a faster interspike interval (*Mwk*/+: 0.14 $\pm$ 0.02 s interspike interval, 1.156 $\pm$ 0.307 nA spike amplitude, $n = 5$; wild-type: 1.36 + 0.48 s interspike interval, 4.188 + 0.1 nA spike amplitude, $n = 3$; mean $\pm$ SEM, $P < 0.05$, unpaired Student's *t* test). Representative examples of Purkinje cells are shown. Spikes are expanded in right panels. (*C*) Upon application of 5 μM DHPG, there was hardly any inward current in wild-type cells (*Upper*), but a clear inward current in *Mwk*/+ Purkinje cells (*Lower*). (*D*) Summary of 5-μM DHPG-evoked currents (*Mwk*/+: 1.635 $\pm$ 0.393 pA, $n = 6$; wild-type: 0.044 $\pm$ 0.03 pA, $n = 5$; mean $\pm$ SEM, $P < 0.01$, unpaired Student's *t* test). (*E*) Transient overexpression of *Mwk* TRPC3 (T635A) but not wild-type TRPC3 significantly induced cell death in NSC-34 cells (25 $\pm$ 0.577 vs. 2 $\pm$ 1.528, $n = 3$; mean $\pm$ SEM, $P < 0.0001$, ANOVA followed by Fisher's PLSD post hoc test). (*F*) In vitro kinase assays using PKCγ with recombinant GST, wild-type TRPC3 GST-S4/S5 linker, and *Mwk* TRPC3 GST-S4/S5 linker (T635A).

significantly induced cell death in various cell lines, including neuronal NSC-34 cells (Fig. 4*E* and data not shown).

A recent study implicated TRPC3 in BDNF-mediated survival of cerebellar granule neurons (17), and so we assessed the cell death of granule neurons derived from both wild-type and *Mwk*/+ mice upon growth factor deprivation or treatment with BDNF, respectively. We did not detect any significant differences in survival between wild-type and *Mwk*/+ granule neurons upon starvation or treatment with BDNF (Fig. S3). These findings, together with our histological observations, suggest that the activating mutation in TRPC3 specifically affects the survival of Purkinje cells in the *Mwk* cerebellum.

We next addressed the question of how the *Mwk* mutation in the S4/S5 linker of TRPC3 might result in the activation of the channel. One mechanism of TRPC3 regulation is phosphorylation by protein kinase C γ (PKCγ), which has been shown to inhibit TRPC3 channel activity (18, 19). Interestingly, threonine 635, the residue mutated in *Mwk*/+ mice, constitutes a conserved putative site for phosphorylation by PKCγ. Using an in vitro kinase assay, we found that PKCγ robustly catalyzed the phosphorylation of the wild-type TRPC3 S4/S5 linker, but failed to phosphorylate the *Mwk* S4/S5 linker in which threonine 635 was replaced with alanine (T635A) (Fig. 4*F*). Thus, the loss of an inhibitory PKCγ-mediated phosphorylation of TRPC3 at threonine 635 may well result in the observed activation of the TRPC3 channel in *Mwk*/+ mice.

Altered Dendritic Development of Mutant Purkinje Cells. Consistent with the observed altered electrophysiology of Purkinje cells,

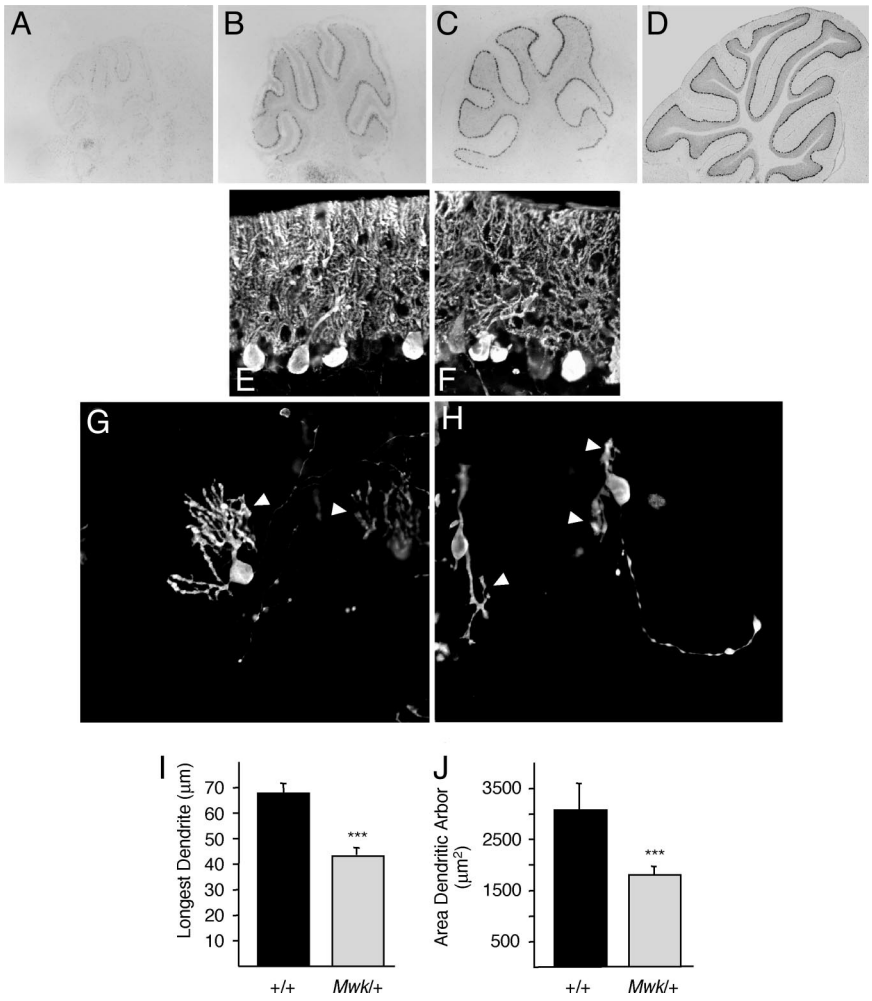

Fig. 5. TRPC3 is a critical regulator of dendritic growth and differentiation in cerebellar Purkinje cells. (*A–D*) In situ hybridization images for *Trpc3* in wild-type mouse cerebellum at 8 days (*A*), 13 days (*B*), 18 days (*C*), and 56 days (*D*) of age. (*E* and *F*) Cerebellar sections of 3-week-old wild-type (*E*) and *Mwk*/+ (*F*) mice subjected to immunohistochemistry using an anti-calbindin antibody. (*G–J*) Organotypic slice cultures (P8 + 12) prepared from wild-type mice (*G*) and *Mwk*/+ (*H*) littermates were stained with an anti-calbindin antibody. Arrowheads indicate dendritic trees. *Mwk*/+ Purkinje cells had a significantly shorter longest dendrite (*I*) (44.8 ± 2.5 μm vs. 74.18 ± 3.6 μm) and significantly reduced areas of the dendritic arborization (*J*) (1358.7 ± 119.9 μm^2 vs. 3487.9 ± 225.14 μm^2). Results shown are representative of 3 independent experiments (mean ± SEM, $n = 59$, $P < 0.0001$, ANOVA followed by Fisher's PLSD post hoc test).

Mwk/+ mice exhibit ataxic behavior long before any Purkinje cell loss is observed, suggesting that the ataxic phenotype is caused by the abnormal functioning of mutant Purkinje cells in the *Mwk* cerebellum. Interestingly, TRPC3 expression starts within the second postnatal week and peaks at 3 weeks postnatally (Fig. 5 *A–D*) (13). It is during this phase that the rapid growth and maturation of Purkinje cell dendrites occurs (20). We therefore set out to investigate whether TRPC3 might play a role in the dendritic development of Purkinje cells. Remarkably, Purkinje cell dendritic arbors appeared less elaborate with fewer branches in cerebellar sections prepared from 3-week-old mutant mice compared with wild-type (Fig. 5 *E* and *F*). To reveal possible quantitative differences in the size and complexity of the dendritic trees, we assessed Purkinje cell morphology in organotypic cerebellar slice cultures from *Mwk*/+ mice and their wild-type littermates. Most wild-type Purkinje cells extended complex dendritic trees in the organotypic slices (Fig. 5*G*). In contrast, the dendritic trees of *Mwk*/+ Purkinje cells were greatly reduced in size and complexity (Fig. 5 *H–J*). Dendritic expansion of *Mwk*/+ Purkinje cells, as measured by the length of the longest dendrite, was decreased by 40% compared with wild-type (Fig. 5*I*). Furthermore, the area of dendritic trees of *Mwk*/+ Purkinje cells was significantly smaller than that of wild-type controls and often reduced to a few stubby branches (Fig. 5*J*). Together, these findings suggest that TRPC3 is a regulator of dendritic growth and arborization in cerebellar Purkinje cells.

Discussion

In this study, we have described a unique dominant mouse model of cerebellar ataxia that displays abnormal Purkinje cell development, dysfunction, and subsequent degeneration due to a point mutation in the TRPC3 nonselective cation channel. Our findings uncover a previously unknown role for TRPC3 in both development and survival of cerebellar Purkinje cells, and provide a unique link between aberrant TRPC3 function and cerebellar ataxia.

Our study sheds light on the important question of how the development of the highly elaborate dendritic trees of Purkinje cells is regulated. One of the key molecules determining Purkinje cell dendritic development is PKCγ (20, 21). However, the PKCγ-mediated signaling pathways that control dendrite morphology remain largely elusive. Both PKCγ and TRPC3 are activated downstream of phospholipase C (PLC)-coupled membrane receptors (19). In vitro studies have shown that PKCγ

GENETICS

inhibits TRPC3 channel activity, thereby providing a negative feedback mechanism (18, 19). Our study suggests that TRPC3 might be a target of PKCγ-mediated phosphorylation at the distinct site of threonine 635. Thus, the absence of the PKCγ-mediated negative feedback on TRPC3 might promote sustained TRPC3 activation and result in limited dendritic arborization in *Mwk* Purkinje cells. Interestingly, activation of class 1 metabotropic glutamate receptors has also been implicated in the inhibition of Purkinje cell dendritic growth as a negative feedback mechanism for limiting the size of the dendritic tree of Purkinje cells after the establishment of a sufficient number of parallel fiber contacts (22). Both mGluR1 and TRPC3 localize to Purkinje cell soma and dendrites during postnatal development (13, 23), and there is now compelling evidence that TRPC3 signals downstream of mGluR1 in cerebellar Purkinje cells (present study and ref. 7). Hence, the PKCγ-mediated inhibitory phosphorylation of TRPC3 may provide the molecular basis for the mGluR1-triggered negative feedback on Purkinje cell dendritogenesis during cerebellar development. Future studies of mGluR1-PKCγ-TRPC signaling in Purkinje cells will help to elucidate the effector molecules that control dendritic development.

The high expression of TRPC3 in Purkinje cells persists into adulthood (Fig. 5*D*) (13), suggesting that TRPC3's function in these neurons extends beyond the regulation of dendritic development. Indeed, a recent study has implicated TRPC3 in the normal synaptic function of Purkinje cells (7). Based on our findings, it is an attractive hypothesis that TRPC3 may also continue to regulate the growth and refinement of Purkinje cell dendritic trees in the adult cerebellar cortex and thereby contribute to synaptic remodeling and plasticity. A unique form of synaptic plasticity in the cerebellum that is critical for motor learning is long-term depression (LTD) in Purkinje cells (24). LTD is mediated by mGluR1 signaling (25, 26), raising the interesting possibility that TRPC3 may play a role in cerebellar LTD and motor learning.

Although we focus in this study on the role of TRPC3 in the cerebellum, the *Mwk* mouse might also provide insight into TRPC3 function in other tissues. TRPC3 is highly expressed in the cerebellum but also found in other nervous and nonnervous tissues, including the heart (27, 28). It will be interesting to characterize the function of TRPC3 in these tissues in the *Mwk* mouse and to determine whether the expression of mutant TRPC3 contributes to the reduced growth of *Mwk* mice and/or the embryonic lethality observed in homozygous *Mwk*/*Mwk* mice.

Our study provides a link between aberrant Purkinje cell development and cerebellar ataxia in the *Mwk* mouse. There is increasing evidence that altered neurodevelopmental processes contribute to neurodegenerative diseases, including Alzheimer's disease, Parkinson's disease, and spinocerebellar ataxia (SCA) (29–31). Interestingly, TRPC3 is downregulated in Purkinje cells in the SCA1 mouse model before the onset of degeneration (32). Furthermore, mutants of PKCγ causing SCA14 fail to phosphorylate TRPC3 (33). In view of our findings, these observations raise the interesting possibility that abnormal TRPC3 function might contribute to different forms of human cerebellar ataxia.

Methods

Plasmids. The GFP-TRPC3 plasmid was kindly provided by J. W. Putney, Jr. TRPC3 was subcloned into the p3xFLAG-CMV-7.1 expression vector (Sigma). The GST-TRP3 S4/S5 plasmid was generated by PCR cloning the residues corresponding to the mouse TRPC3 S4/S5 linker (bp 1855–1923) into pGEX-4T-3 (Amersham Pharmacia Biotech). The *Mwk* point mutation (T635A) was made by site-directed mutagenesis using the QuikChange Site-Directed Mutagenesis Kit (Stratagene). All constructs were verified by sequencing.

Mice. The founder mouse carrying the *Mwk* mutation was generated in a large-scale ENU mutagenesis program at the Medical Research Council center in Harwell, U.K. (6). Briefly, male BALB/cAnN mice were mutagenized and crossed to normal C3H/HeH females, and the F1 progeny were screened for a variety of defects, including gait abnormalities. The *Mwk*/+ colony was maintained by repeated backcrossing to C3H/HeH. All animal studies were carried out under the ''Responsibility in the Use of Animals for Medical Research'' guidelines issued by the Medical Research Council in 1993, and Home Office Project Licenses 30/2198 and 30/2306.

Genetic Mapping and Mutation Detection. Mutant progeny were identified by their ataxic behavior. A genome scan using 72 polymorphic markers was performed with 13 affected progeny and showed linkage to Mmu3. For high-resolution genetic mapping, 124 mutant mice were screened using published microsatellite markers *D3Mit90*, *D3Mit93*, *D3Mit203*, *D3Mit268*, *D3Mit167*, *D3Mit273*, *D3Mit206*, *D3Mit180*, *D3Mit168*, *D3Mit331*, *D3Mit239*, *D3Mit21*, *D3Mit169*, *D3Mit295*, *D3Mit273*, *D3Mit3*, *D3Mit306*, and *D3Mit333*. Polymorphic differences were visualized on 1%–4% agarose gels. Mutation detection within the nonrecombinant region was performed by direct sequencing.

Behavioral Analysis. Footprint analysis of 2-month-old mice was carried out as described (8, 34). Briefly, hind feet of mice were coated with nontoxic ink, and mice were allowed to walk through a tunnel (50 cm long, 9 cm wide, 8 cm high). Then the footprint patterns made on paper lining the floor were analyzed. Gait width, the average lateral distance between opposite left and right steps, was determined by measuring the perpendicular distance of a given step to a line connecting its opposite preceding and succeeding steps. The alternation coefficient, a value describing the uniformity of step alternation, was calculated by determining the mean of the absolute values of 0.5 minus the ratio of right-left step distance to right-right step distance for every right-left step pair. A perfect tandem alternating gait in which all alternate steps fell exactly equidistant between the preceding and succeeding opposite steps would have a calculated alternation coefficient of zero. Conversely, a shuffle gait in which all alternate steps fell exactly beside the preceding opposite steps would have a calculated value of 0.5. For the static rod test, 2-month-old mice were placed on the protruding end of a wooden bar (28 mm diameter, 60 cm length) that was fixed to solid support at the other end, approximately 60 cm above a padded surface. Mice were placed on the protruding end, facing away from the support, and the time taken to turn around and for all 4 paws to reach the supported end and the latency time to fall were recorded up to a maximum score of 180 seconds.

Immunohistochemistry. Brains were removed from mice transcardially perfused with 4% paraformaldehyde and embedded in paraffin wax. Cerebellar sections of 10 μm were stained with rabbit anti-calbindin D28K (Swant) at a 1:15,000 dilution for 2 days at 4 °C as previously described (35).

Real-Time PCR. RNA was extracted from 3-week-old mouse cerebella using the RNeasy Kit (Qiagen) and reversed transcribed into cDNA using oligo(dT) primers and Expand Reverse Transcriptase (Roche) under standard conditions. qRT-PCR was performed in Fast SYBR Green Master Mix (Applied Biosystems) on a StepOnePlus Real-Time PCR System (Applied Biosystems) according to the manufacturer's instructions. TRPC3 and TRPC1 levels were quantified and normalized against coamplified calbindin levels using standard DDCt techniques. Primers were: AAAGAAAACGATGAGGTGAATGAAG (TRPC3 forward), CATAACGAAGGCTGGAGATATCCT (TRPC3 reverse), TGCTCGCATACCTCGAAAGG (TRPC1 forward), TCTCGTCTCTCTTTTGCTTCAAGTT (TRPC1 reverse), TGTGTGGGAAAGAGTTCAATAAGG (Calbindin forward), TCCAGCTCATTTTCATCTATGTATCC (Calbindin reverse).

Preparation of Cerebellar Lysates and Immunoblotting. Three-week-old mice were killed, and cerebella were dissected out and kept on ice. Protein extracts from cerebella were prepared by 30-s sonication in RIPA buffer (50 mM Tris, 150 mM NaCl, 1% Nonidet P40, 0.5% sodium dexycholate, 0.1% SDS, 1× Complete Protease Inhibitors [Roche]), followed by 10-min incubation on ice and 15-min centrifugation at 14,000 *g* at 4 °C. Fifty micrograms of lysates were analyzed by SDS/PAGE and immunoblotting with antibodies against TRPC3 (Alomone Labs) and actin (Abcam).

Electrophysiology. Mice (P20-P22; 20–22 days old) were decapitated following cervical dislocation, and the cerebellar vermis was dissected out and cooled in ice-cold bicarbonate-buffered saline (BBS) (125 mM NaCl, 2.5 mM KCl, 26 mM $NaHCO_3$, 1.25 mM NaH_2PO_4, 2 mM $CaCl_2$, 1 mM $MgCl_2$, and 10 mM glucose [pH 7.4 when oxygenated with carbogen]). Sagittal slices of 200 μm were cut using

a vibratome and incubated in oxygenated BBS at room temperature for at least 40 min before their use in experiments. Tight-seal whole-cell recordings were obtained from Purkinje cells using an EPC9/2 patch-clamp amplifier (Heka Electronics). Patch pipettes had resistances of 2–3 MΩ with the internal (150 mM CsCl, 10 mM Hepes, 4 mM Na-ATP, 0.4 mM Na-GTP, 4.6 mM $MgCl_2$ [pH adjusted to 7.3 with CsOH]) and extracellular solutions (BBS). Series resistance did not exceed 10 MΩ and was typically between 5 and 6 MΩ. Capacitative currents were cancelled and series resistance was compensated by between 50% and 60%. A 63× water immersion objective was used for visualization of the slices during experiments. Experiments were performed at room temperature and slices were continuously perfused with oxygenated BBS + 0.25 μM TTX at a rate of >7 ml/min. DHPG was applied to the slice by dissolving prepared stock solutions into BBS to the desired concentration. Only 1 cell per slice was used for each experiment to avoid contamination of the results by potential long-term side effects of DHPG.

Cell-Survival Assays. For survival assays in NSC-34 cells, cells were transfected using Fugene 6 Transfection Reagent (Roche) according to the manufacturer's instructions. Twenty-four hours after transfection, cells were fixed with 4% paraformaldehyde and subjected to immunofluorescence. Cell survival and death were assessed in GFP-expressing cells based on the nuclear morphology as determined using the DNA dye DAPI (Vector Laboratories). Cell counts were carried out in a blinded manner ($n = 100$ cells per condition). For survival assays of cerebellar granule neurons, primary cerebellar granule neurons were prepared from 5-day-old mice (P5) as described (36). After 4 days in culture (P5 + 4), cultures were left untreated in conditioned media, or incubated in basal medium eagle (BME) in the presence or absence of 50 ng/ml BDNF (Sigma) for 48 h. Subsequently, cells were fixed, and cell survival and death were assessed as described previously.

In Vitro Kinase Assays. In vitro PKCγ kinase assays were carried out according to the manufacturer's protocol (Upstate Biotechnology). Briefly, recombinant active PKCγ kinase was incubated with 5 μg recombinant GST, wild-type GST-S4/S5 linker, or *Mwk* GST-S4/S5 linker for 30 min at 30 °C in 20 mM Hepes/NaOH (pH 7.4), 0.1 mg/ml phosphatidylserine, 0.01 mg/ml diacylglycerol, 100 μM $CaCl_2$, 100 μM ATP, and 0.5 μCi of [γ-^{32}P] ATP. Kinase reactions were analyzed by SDS-PAGE, Coomassie Blue staining, and autoradiography.

In Situ Hybridization. In situ hybridization for *Trpc3* was carried out on 12-μm cryosections from wild-type male C3H/HeH brains of the indicated ages. Primers for riboprobe amplification by RT-PCR were: ACTCAGTGAGAAACTGAACCCC and CTCAGTGATGGTCTCTCGTCTG. Digoxigenin-labeled riboprobe synthesis and hybridization was carried out as described previously (35). All sections were developed for 24 h. A sense strand negative control probe gave no detectable signal.

Organotypic Slice Cultures. For cerebellar organotypic slice cultures, 8-day-old (P8) mouse pups were decapitated following cervical dislocation and their brains were removed. The cerebellum was dissected and the meninges were removed. Sagittal slices of 400 μm were cut using a McIllwain Tissue Chopper. Slices were separated, transferred onto 0.4-μm permeable membranes (Millicell-CM, Millipore), and cultured on a layer of medium (MEM with 25 mM Hepes, 25% horse serum, 6.5 mg/ml D-glucose, 2 mM glutamine, penicillin/streptomycin) in a humidified atmosphere with 5% CO_2 at 37 °C. The medium was changed every 2–3 days. After 12 days (P8 + 12), slices were fixed in 4% paraformaldehyde followed by methanol permeabilization. Slices were blocked in PBS containing 0.3% Triton-X and 3% goat serum for 1 h at room temperature and incubated with rabbit anti-calbindin antibody (1:5,000) (Swant) for 2 nights at 4 °C followed by incubation with Alexa Fluor 488 donkey anti-rabbit antibody (1:2,000) (Invitrogen). For the quantification of Purkinje cell dendritic morphology, images of Purkinje cells were taken at 40× magnification, and dendritic length and area were analyzed using the Axiovision 4.3 software (Zeiss). Cells were acquired from 3 independent experiments.

Statistical Analysis. All data are represented as mean ± SEM. All statistical analyses were done using the software programs Statview and Instat. For pairwise comparisons, Student's *t* test was used. For comparisons within multiple data sets, ANOVA was used, and *P* values were calculated using the Fisher's protected least significance difference (PLSD) posthoc test.

ACKNOWLEDGMENTS. We thank Dilair Baban, Luis Paixao, and Nick Parkinson for technical assistance and helpful discussions, and Sian Polley, Rachel Kendall, and Denise Jelfs for animal work support. This work was supported by the U.K. Medical Research Council and the U.K. Motor Neuron Disease Association. E.B. is a fellow of the International Human Frontier Science Program Organization.

1. Duenas AM, Goold R, Giunti P (2006) Molecular pathogenesis of spinocerebellar ataxias. *Brain* 129:1357–1370.
2. Klockgether T (2000) Recent advances in degenerative ataxias. *Curr Opin Neurol* 13:451–455.
3. Taroni F, DiDonato S (2004) Pathways to motor incoordination: The inherited ataxias. *Nat Rev Neurosci* 5:641–655.
4. Matilla-Duenas A (2008) The highly heterogeneous spinocerebellar ataxias: From genes to targets for therapeutic intervention. *Cerebellum* 7:97–100.
5. Lim J, et al. (2006) A protein-protein interaction network for human inherited ataxias and disorders of Purkinje cell degeneration. *Cell* 125:801–814.
6. Nolan PM, et al. (2000) Implementation of a large-scale ENU mutagenesis program: Towards increasing the mouse mutant resource. *Mamm Genome* 11:500–506.
7. Hartmann J, et al. (2008) TRPC3 channels are required for synaptic transmission and motor coordination. *Neuron* 59:392–398.
8. Oliver PL, Keays DA, Davies KE (2007) Behavioural characterisation of the robotic mouse mutant. *Behav Brain Res* 181:239–247.
9. Eder P, Poteser M, Groschner K (2007) TRPC3: A multifunctional, pore-forming signalling molecule. *Handb Exp Pharmacol* 179:77–92.
10. Flockerzi V (2007) An introduction on TRP channels. *Handb Exp Pharmacol* 179:1–19.
11. Ramsey IS, Delling M, Clapham DE (2006) An introduction to TRP channels. *Annu Rev Physiol* 68:619–647.
12. Venkatachalam K, Montell C (2007) TRP channels. *Annu Rev Biochem* 76:387–417.
13. Huang WC, Young JS, Glitsch MD (2007) Changes in TRPC channel expression during postnatal development of cerebellar neurons. *Cell Calcium* 42:1–10.
14. Kim SJ, et al. (2003) Activation of the TRPC1 cation channel by metabotropic glutamate receptor mGluR1. *Nature* 426:285–291.
15. Strubing C, Krapivinsky G, Krapivinsky L, Clapham DE (2003) Formation of novel TRPC channels by complex subunit interactions in embryonic brain. *J Biol Chem* 278:39014–39019.
16. Singh BB, et al. (2004) VAMP2-dependent exocytosis regulates plasma membrane insertion of TRPC3 channels and contributes to agonist-stimulated Ca2+ influx. *Mol Cell* 15:635–646.
17. Jia Y, Zhou J, Tai Y, Wang Y (2007) TRPC channels promote cerebellar granule neuron survival. *Nat Neurosci* 10:559–567.
18. Trebak M, et al. (2005) Negative regulation of TRPC3 channels by protein kinase C-mediated phosphorylation of serine 712. *Mol Pharmacol* 67:558–563.
19. Venkatachalam K, Zheng F, Gill DL (2003) Regulation of canonical transient receptor potential (TRPC) channel function by diacylglycerol and protein kinase C. *J Biol Chem* 278:29031–29040.
20. Kapfhammer JP (2004) Cellular and molecular control of dendritic growth and development of cerebellar Purkinje cells. *Prog Histochem Cytochem* 39:131–182.
21. Schrenk K, Kapfhammer JP, Metzger F (2002) Altered dendritic development of cerebellar Purkinje cells in slice cultures from protein kinase Cgamma-deficient mice. *Neuroscience* 110:675–689.
22. Sirzen-Zelenskaya A, Zeyse J, Kapfhammer JP (2006) Activation of class I metabotropic glutamate receptors limits dendritic growth of Purkinje cells in organotypic slice cultures. *Eur J Neurosci* 24:2978–2986.
23. Lopez-Bendito G, Shigemoto R, Lujan R, Juiz JM (2001) Developmental changes in the localisation of the mGluR1alpha subtype of metabotropic glutamate receptors in Purkinje cells. *Neuroscience* 105:413–429.
24. Ito M (2002) The molecular organization of cerebellar long-term depression. *Nat Rev Neurosci* 3:896–902.
25. Aiba A, et al. (1994) Deficient cerebellar long-term depression and impaired motor learning in mGluR1 mutant mice. *Cell* 79:377–388.
26. Ichise T, et al. (2000) mGluR1 in cerebellar Purkinje cells essential for long-term depression, synapse elimination, and motor coordination. *Science* 288:1832–1835.
27. Riccio A, et al. (2002) mRNA distribution analysis of human TRPC family in CNS and peripheral tissues. *Brain Res Mol Brain Res* 109:95–104.
28. Watanabe H, et al. (2008) TRP channel and cardiovascular disease. *Pharmacol Ther* 118:337–351.
29. Bothwell M, Giniger E (2000) Alzheimer's disease: Neurodevelopment converges with neurodegeneration. *Cell* 102:271–273.
30. Serra HG, et al. (2006) RORalpha-mediated Purkinje cell development determines disease severity in adult SCA1 mice. *Cell* 127:697–708.
31. Wexler EM, Geschwind DH (2007) Out FOXing Parkinson disease: Where development meets neurodegeneration. *PLoS Biol* 5:e334.
32. Lin X, et al. (2000) Polyglutamine expansion down-regulates specific neuronal genes before pathologic changes in SCA1. *Nat Neurosci* 3:157–163.
33. Adachi N, et al. (2008) Enzymological analysis of mutant protein kinase Cgamma causing spinocerebellar ataxia type 14 and dysfunction in Ca2+ homeostasis. *J Biol Chem* 283:19854–19863.
34. Clark HB, et al. (1997) Purkinje cell expression of a mutant allele of SCA1 in transgenic mice leads to disparate effects on motor behaviors, followed by a progressive cerebellar dysfunction and histological alterations. *J Neurosci* 17:7385–7395.
35. Isaacs AM, et al. (2003) A mutation in Af4 is predicted to cause cerebellar ataxia and cataracts in the robotic mouse. *J Neurosci* 23:1631–1637.
36. Becker EB, et al. (2004) Characterization of the c-Jun N-terminal kinase-BimEL signaling pathway in neuronal apoptosis. *J Neurosci* 24:8762–8770.